NJC

Accepted Manuscript

This article can be cited before page numbers have been issued, to do this please use: S. V. Smitha, S. S S, A. M. Peer, B. N. Nair and H. U. N. Saraswathy, *New J. Chem.*, 2018, DOI: 10.1039/C7NJ05174C.

ROYAL SOCIETY OF CHEMISTRY

rsc.li/njc

View Article Online
DOI: 10.1039/C7NJ05174C

Journal Name

ARTICLE

Ormosil-ZrO_2 hybrid nanocomposites and coatings on aluminium alloy for corrosion resistance; A sol-gel approach

Received 00th January 20xx,
Accepted 00th January 20xx

DOI: 10.1039/x0xx00000x

www.rsc.org/

V. S. Smitha,[a]* S. S. Syamili,[a] A. Peer Mohammed,[a] Balagopal N Nair [b,c] and U. S. Hareesh*[a,d]

Corrosion resistant coatings are prepared from a hybrid nanocomposite aerogel derived from the tri-functional silanes, methyl trimethoxy silane (MTMS), glycidyloxy propyl trimethoxy silane (GPTMS) and from zirconium isopropoxide (ZIP) precursor which acts as an inorganic nano-dispersion in the organically modified silane (ORMOSIL) matrix. A series of hybrid compositions of MTMS and GPTMS are prepared in which the amount of ZIP was varied. The variations in the pH, viscosity and the gelation time of the prepared compositions are monitored. The wet alcogels thus obtained are homogenized in a solvent by an ultrasonicator followed by coating the suspension on aluminum alloy and glass substrates using a dip coating unit. The prepared coatings are further dried and annealed at 400 °C for 1h. The wet alcogels are also dried under ambient conditions for seven days resulting in hybrid nanocomposite aerogel monoliths and are calcined at 400 °C. The hybrid nanocomposites and coatings are further characterized by X-ray diffraction Analysis, Fourier Transform Infrared Spectroscopy, BET Surface Area Analysis, X-ray Photoelectron Spectroscopy, Scanning Electron Microscopy (SEM), Atomic Force Microscopy (AFM), UV-Visible spectroscopy, potentiodynamic polarization and EIS measurements. The hybrid nanocomposite coated aluminum alloy shows an enhanced corrosion protection when compared to the uncoated aluminum alloy. The anticorrosive feature of the ORMOSIL-ZrO_2 hybrid nanocomposite coating makes them an important candidate in the field of protective environment resistant coatings.

Introduction

Functional materials are widely recognized as materials possessing unique functions and are suitable for a variety of applications.[1, 2] Inorganic-organic hybrids constitutes an important class of functional material that finds promising applications as functional coatings, a significant technology for industry as well as society in the current environmental scenario.[3-5] Organically modified silicates (ORMOSIL) are sol-gel based inorganic-organic hybrid systems formed through the hydrolysis and condensation of organically modified silanes with traditional alkoxide precursors.[6, 7] ORMOSILs favour the formation of interpenetrating organic-inorganic networks that reinforces the structure and thereby improving the mechanical properties of the hybrid system.[8, 9] In an ORMOSIL based hybrid system there occurs a synergism between the thermal stability of the silica block and the flexibility of the polymer chain.[10, 11] The superior properties such as tunable porosity and good adhesion on different substrates compared to conventional organic or inorganic coatings make ORMOSILs a perfect material of choice for the development of functional coatings.

Functional ORMOSIL coatings are widely used for imparting corrosion resistance[12] to aluminium alloys as they are highly susceptible to oxidation and pitting corrosion in aggressive environments.[13, 14] Incorporation of functionalized silica nanoparticles into silica/EDTPO matrix is reported to provide long-term corrosion protection to aluminium alloy due to the enhancement of barrier properties.[15] Multilayer hybrid sol-gel coatings on stainless steel substrate based on a TEOS-GPTMS system produces uniform and homogeneous coatings with enhanced corrosion resistance as reported by Caballero et al.[16] Incorporating inorganic particles into a hybrid ORMOSIL matrix[17] may further result in enhanced corrosion resistance features due to the nanocomposite effect.[18] The addition of clay to silica-based sol-gel films protects aluminium from corrosion as reported by Dalmoro et al.[19] Integration of zirconia nanoparticles into a hybrid matrix enhances several material functionalities because of its high mechanical strength, temperature resistance and chemical stability.[20] Ruiz et al. has

[a] Materials Science and Technology Division, CSIR-National Institute for Interdisciplinary Science and Technology, Industrial Estate P. O., Trivandrum, Pin Code-695019, India
[b] Nanochemistry Research Institute, Department of Chemistry, Curtin University, GPO Box U1987, Perth, Western Australia 6845, Australia
[c] R&D Centre, Noritake Company Limited, 300 Higashiyama, Miyoshi, Aichi 470-0293, Japan
[d] Academy of Scientific and Innovative Research, Delhi-Mathura Road, New Delhi 110025, India
Electronic Supplementary Information (ESI) available: [Photographs of hybrid aerogel monoliths and coatings]. See DOI: 10.1039/x0xx00000x

View Article Online
DOI: 10.1039/C7NJ05174C

studied the microabrasion-corrosion features of SiO_2-TiO_2-ZrO_2 coatings on stainless steel and found that the coatings were abrasion and corrosion resistant.[21] Thus there exists a lot of scope for the development of corrosion resistant smart functional coatings on alloys suitable for industrial applications.[22]

In the present work, transparent, corrosion resistant coatings were prepared from a hybrid nanocomposite aerogel derived from two tri-functional silanes such as MTMS, an alkyl functional silane and GPTMS, the one with epoxy functionality and from zirconium isopropoxide (ZIP) precursor which acts as an inorganic nanodispersant in the ORMOSIL matrix. The nanostructured interconnected network morphology of the ORMOSIL based hybrid nanocomposite aerogel coating can offer high levels of transparency and by tuning the hydrolysis condensation parameters, one can have a good control over the thickness and porosity and hence it does not require any additional surface treatments for practical applications. The overall advantage of using the mixed precursor MTMS/GPTMS for the synthesis of hybrid aerogel coatings in the present work is the enhanced adhesion and corrosion resistance features of the MTMS/GPTMS hybrid aerogel particles to the substrate used for coating.[23] The introduction of epoxide groups into the coating by addition of a silane having epoxide group for synthesis can significantly improve adherence features as reported by Wang et al.,[24] and the better adhesion stability of the MTMS/GPTMS aerogel particles on to coated substrate is clearly demonstrated in a previous work reported by the author.[25] To the best of our knowledge, the effect of zirconia on the corrosion resistance of hybrid aerogel coatings based on MTMS and GPTMS has not been carried out yet. The anticorrosive feature of the ORMOSIL-ZrO_2 hybrid nanocomposite coating ensures the applicability of such coatings as protective environment resistant coatings.

Results and discussion

The structure and properties of an aerogel is greatly influenced by the pH of the sol-gel system. An acid catalyzed hydrolysis (pH < 5) is carried out in the present work which limits the unfavourable condensation reactions during hydrolysis stage.[26] The condensation reaction on the network former silicon atoms [Si–(O–Si)] are usually favoured at high pH[26] and hence a base catalyzed condensation reaction was performed. During the acid catalyzed hydrolysis, alkoxide groups (OR) are replaced with hydroxyl groups (OH) while the silanol groups will condense together to form siloxane bonds and alcohol (ROH) or water in the subsequent condensation reaction.[27] The relative rate of hydrolysis and condensation reactions was monitored through changes in pH and viscosity of the ORMOSIL compositions. The variation in the pH of the various compositions prepared with respect to time after the addition of varying amounts of zirconium isopropoxide (ZIP) and the basic catalyst is presented below in Fig. 1 and the corresponding gelation times of the hybrids are provided in Table 1.

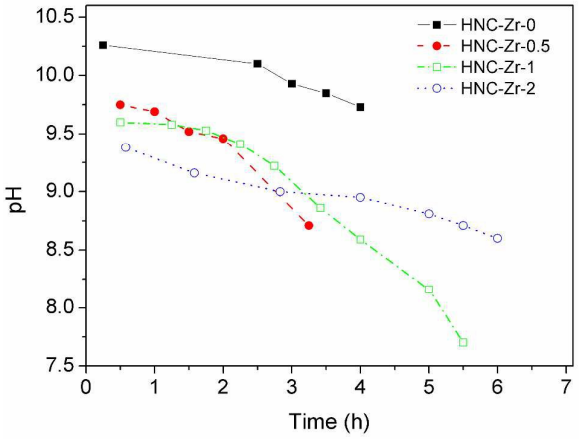

Fig. 1. Variation in the pH of the ORMOSIL-ZrO_2 hybrid compositions with respect to time after the addition of basic catalyst.

Table 1. Gelation time for the hybrid nanocomposites with respect to the variation in the ZIP concentration.

Sample	MTMS: ZIP	NH_4OH: NH_4F	Gelation time (h)
HNC-Zr-0	1: 0	1: 0.1	4
HNC-Zr-0.5	1: 0.5	1: 0.1	4
HNC-Zr-1	1: 1	1: 0.1	6
HNC-Zr-2	1: 2	1: 0.1	72

The initial pHs of the compositions were decreased with respect to an increase in the ZIP concentration and the pH of the samples was found to decrease significantly near to the gelation point. The changes in the pH of the composition containing high ZIP concentration (MTMS: ZIP 1: 2) was not significant for the initial 6 hours as the gelation time of the composition was very high (72 h). The variation in the viscosity of the ORMOSIL-ZrO_2 hybrid compositions with respect to time after the addition of varying amounts of ZIP and basic catalyst is presented in Fig. 2.

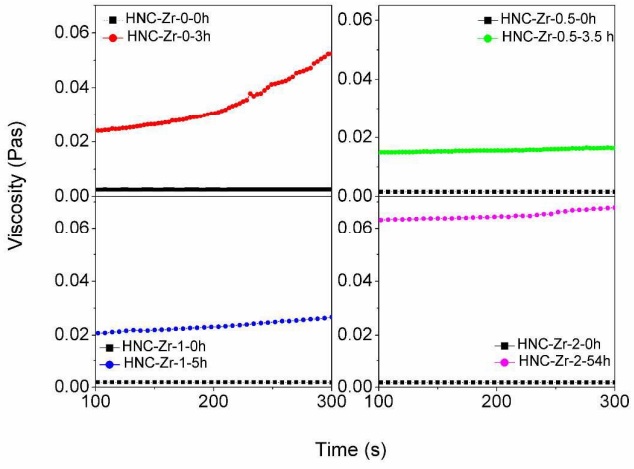

Fig. 2. Variation in the viscosity of the ORMOSIL-ZrO_2 hybrid compositions with respect to time after the addition of ZIP and basic catalyst.

View Article Online
DOI: 10.1039/C7NJ05174C

An increase in the viscosity of the samples was observed towards the gelation point. The increase in the viscosity with time is due to the progress of condensation reactions in the solution which increases the number of siloxane bonds while reducing the number of silanol and alkoxy groups.[28] Also, the gelation time was found to increase with respect to increased zirconia concentration and a twelve fold increase in the gelation time was observed when there is a change in ZIP ratio from 1 to 2. The variation in the pH, viscosity and gelation times for the hybrid compositions is thus attributed to the variation in the extent of condensation reaction due to the difference in the concentration of ZIP. The hydrolysis condensation reactions happening in the hybrid composition containing ZIP is presented in Scheme 1.

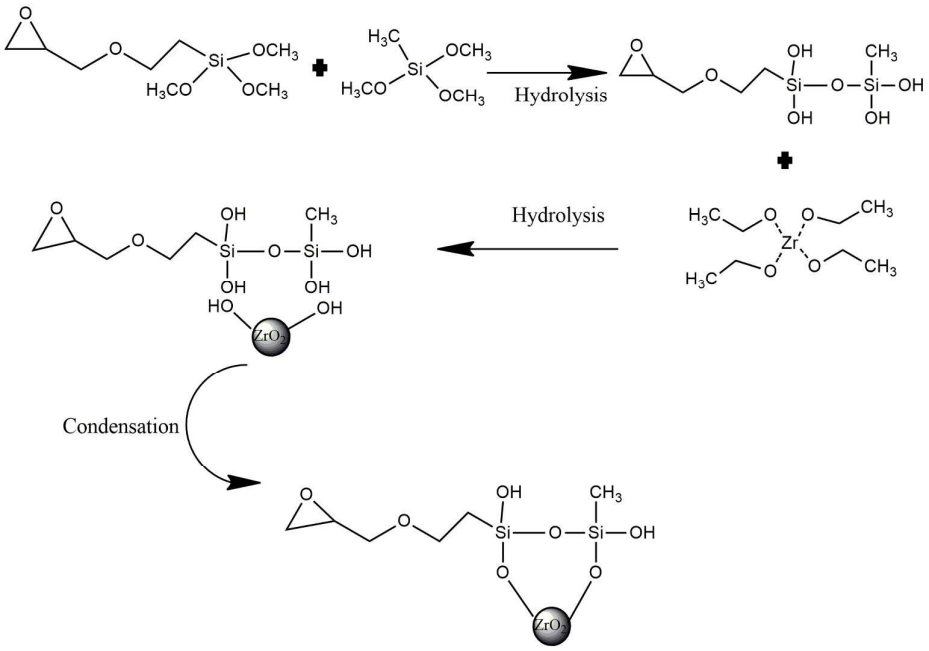

Scheme 1. Schematic representation of the hydrolysis condensation reaction in the inorganic-organic hybrid composition.

The obtained wet alcogels were finally dried under ambient conditions for about seven days to get aerogel monoliths (Fig. S1). The dried gel samples are further calcined at 400 °C and the crystalline and textural features are studied. X-ray diffraction patterns of the hybrid nanocomposite aerogel calcined at 400 °C is provided in Fig. 3 which indicates the semicrystalline nature.

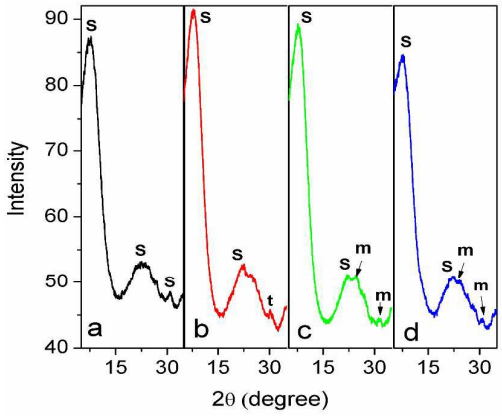

Fig. 3. Wide angle X-ray scattering (WAXS) of (a) HNC-Zr-0 (b) HNC-Zr-0.5 (c) HNC-Zr-1 and (d) HNC-Zr-2, all calcined at 400 °C. ('s' represents the peaks for oligomeric silesquioxane structures, 't' and 'm' represents peaks for tetragonal and monoclinic phases of zirconia respectively).

The presence of the intense first peak at around 7.5 ° suggests the formation of ordered domains inside the hybrid organosilicate network.[29] ORMOSIL based hybrid materials are known to show diffraction peaks in the region 2θ< 10 ° and can be directly related to the organosilane ratio[30] indicating the formation of oligomeric structures during the network formation. The peaks at around 22 ° and 31 ° could also be related to oligomeric units.[31] The organic groups present in trialkoxysilane precursors pose steric hindrance favoring intramolecular reactions leading to the formation of silsesquioxane structures. The hybrid nanocomposites of zirconia exhibits peaks for tetragonal and monoclinic phases of zirconia as evidenced by the peaks at ~30.17 ° for tetragonal zirconia[32] [JCPDS No. 81-1544, (1 0 1) plane] for the HNC-Zr-0.5 and peaks at 24.2 ° and 31.5 ° for monoclinic zirconia[33] [JCPDS Card No: 00-037-1484 (1 1 1) and (0 1 1) planes] for HNC-Zr-1 and HNC-Zr-2 calcined at 400 °C.

The textural features of the samples heat treated at 400 ºC are provided in Table 2. With ZIP addition, the BET surface area of the hybrid nanocomposites was found to increase. The hybrid nanocomposites with MTMS: ZIP ratio1: 0.5 and 1: 1 resulted in lower pore size of 2.1 nm. Further addition of ZIP resulted in slight decrease in the BET surface area. The microporosity in the samples increased with respect to ZIP addition which can be

View Article Online
DOI: 10.1039/C7NJ05174C

attributed to the incorporation of zirconia nanoparticles in the silica network as demonstrated in Scheme 2 below. A pore size reduction was observed in a similar work on silica-zirconia xerogel with increased zirconia loading by Alfaya et al.[34]

Table 2. Textural features of the ORMOSIL-ZrO_2 hybrid nanocomposite aerogel samples calcined at 400 °C.

Sample	Surface Area ($m^2\ g^{-1}$)	Total Pore volume ($cm^3\ g^{-1}$)	Micropore volume ($cm^3\ g^{-1}$)	Mesopore volume ($cm^3\ g^{-1}$)	Pore diameter (nm)
HNC-Zr-0	334.2	0.2300	0.0665	0.1635	2.7
HNC-Zr-0.5	346.3	0.1824	0.0946	0.0878	2.1
HNC-Zr-1	359.4	0.1922	0.0973	0.0949	2.1
HNC-Zr-2	329.3	0.1845	0.1013	0.0832	2.2

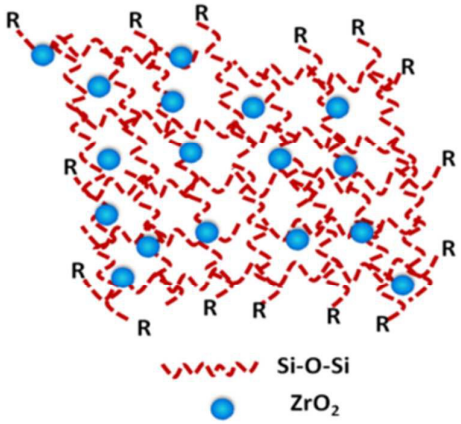

Scheme 2. Schematic showing the entrapped ZrO_2 particles in the ORMOSIL network.

The FTIR analysis of the hybrid nanocomposites calcined at 400 °C was carried out and the results are provided in Fig. 4. Peaks in the range 1000–1100 cm^{-1} are attributed to Si–O–Si bonds.[35] The peak at ~1275 cm^{-1} indicates characteristic vibration bands for -CH_3 bonded to silicon and the one at ~780 cm^{-1} corresponds to Si–C bonds.[36] Peaks at 440 cm^{-1} corresponds to Zr-O vibrations.[37, 38] However, an Si–O–Zr band at ~950 cm^{-1} is indicative of an extended interface between Si and Zr nanodomains.[39] For well-dispersed zirconia on silica, Dang et al.[40] have observed a band at 945 cm^{-1} from IR spectra and attributed this vibration to the possible formation of Si–O–Zr linkages that arises as a result of possible substitution of zirconium in the Si–O–Si linkages.

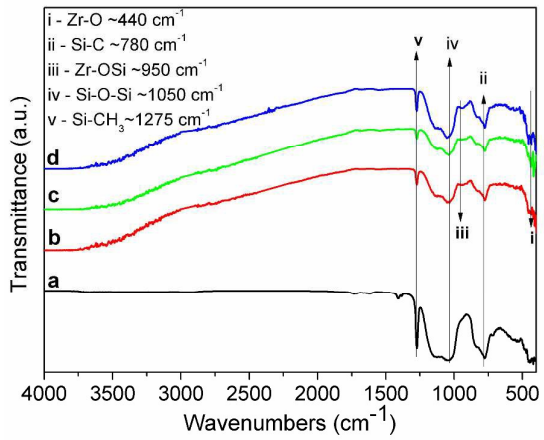

Fig. 4. FTIR spectra of (a) HNC-Zr-0 (b) HNC-Zr-0.5 (c) HNC-Zr-1 and (d) HNC-Zr-2, all calcined at 400 °C.

SEM and EDX analysis of the hybrid nanocomposite HNC-Zr-0.5 calcined at 400 °C is given below (Fig. 5). SEM image of the hybrid nanocomposite reveals the presence of ~25 nm particles with inter-particle porosity and the EDX analysis further confirms the presence of elements such as Si, C, O and Zr.

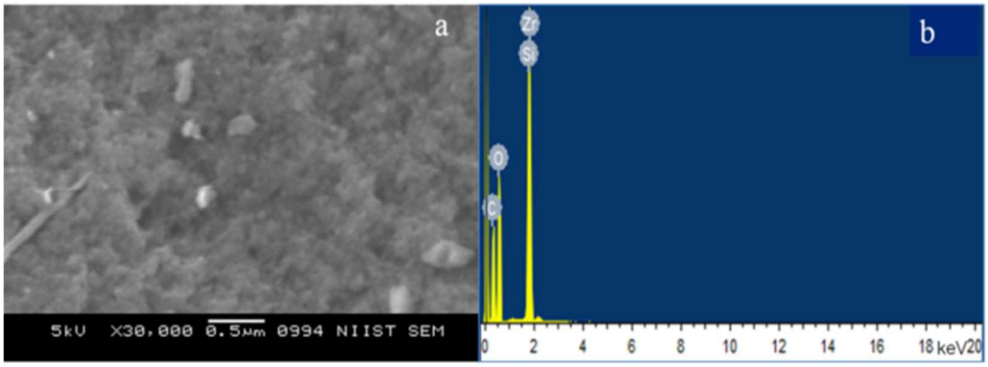

Fig. 5. (a) SEM and (b) EDX analysis of the hybrid nanocomposite HNC-Zr-0.5 calcined at 400 °C.

View Article Online
DOI: 10.1039/C7NJ05174C

Journal Name

ARTICLE

XPS survey spectrum and the deconvoluted C-1s, O-1s and Si-2p spectra of HNC-Zr-0.5 calcined at 400 °C is shown in Fig. 6. Characteristic peaks of Si (2s, 2p), Zr (3d), C (1s) and O (1s) was observed in the survey spectra for the hybrid nanocomposite.

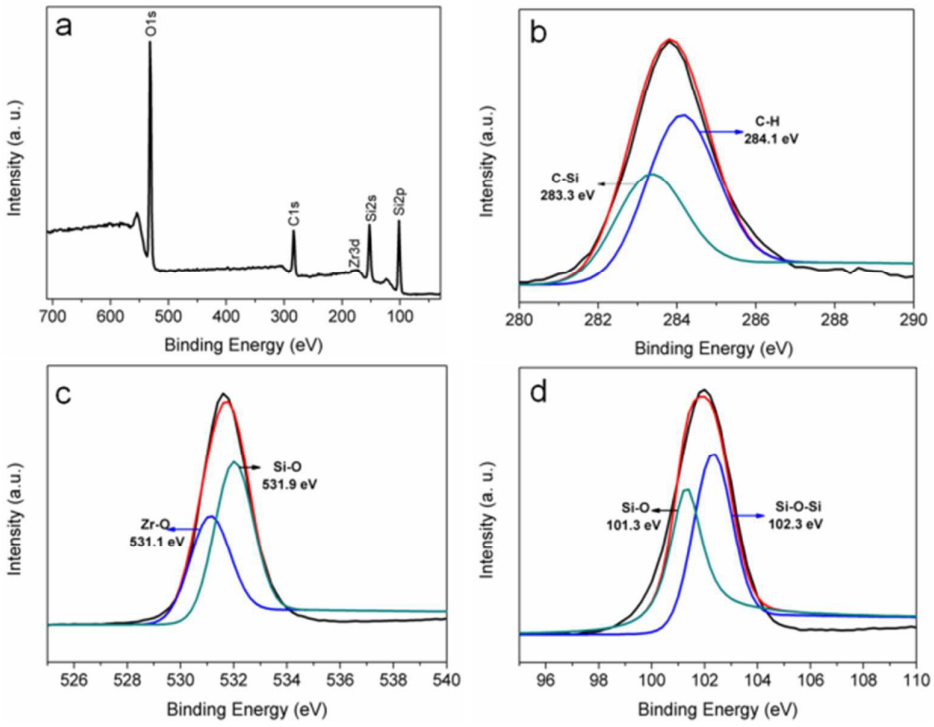

Fig. 6. (a) XPS survey spectrum and the deconvoluted (b) C-1s, (c) O-1s and (d) Si-2p spectra of HNC-Zr-0.5 calcined at 400 °C.

The formation of zirconium oxide (ZrO_2) during the hydrolysis and condensation process was confirmed by the detection of Zr (3d) and O (1s) peaks.[41] The presence of Si 2p and 2s peaks located at 102.3 eV and 152.5 eV, respectively, confirms the formation of a siloxane/silicate network (Si-O-Si bonds).[41, 42] The C1s spectra was deconvoluted into two component peaks with binding energy 284.1 eV corresponding to alkyl groups, (C–H)[43] and 283.3 eV corresponding to C-Si bonds[44] which contributes to the thermal stability of the material. XPS spectra of the O 1s core level was clearly divided into two components centred at 531.1 and 531.9 eV, respectively. The low binding energy peak at 531.1 eV is related to the O–Zr peak[45] and the high binding energy peak centered at 531.9 eV is due to O-Si peak.[46] The deconvoluted Si 2p spectra showed two peaks at 101.3 eV and 102.3 eV which can be assigned to Si^{1+} and Si^{2+} respectively. The contribution of Si^{2+} is more in the sample indicating more Si_2O than SiO, consequently increasing the Si-O-Si bonds which corresponds to a more cross linked structure.[44] The deconvoluted Zr 3d spectra as provided in Fig. S2 shows two peaks centered at 182.4 eV and 181.3 eV. The peak at 182.4 eV can be assigned to Zr^{4+} species of the zirconium oxide phase and the one at 181.3 eV to the Zr^{2+} species.[47] The existence of different zirconium oxide species indicates that ligands around the Zr cations may be different indicating the presence of Zr-OH and Zr-O-Si bonds in the system.[48]

In order to study the functional properties of the prepared ORMOSIL-ZrO_2 hybrid nanocomposites, thin coatings were prepared on polished aluminium substrates and microscopic glass slides by dip coating method and the prepared coatings were annealed at 400 °C for further characterizations. The photographs of the hybrid nanocomposite coated aluminium alloy and glass substrates after calcination at 400 °C are provided (Fig. S3) and the coatings prepared on glass substrates appeared to be transparent. Electrochemical impedance analysis

View Article Online
DOI: 10.1039/C7NJ05174C

of the hybrid nanocomposite coated aluminium alloys were carried out further in 3.5 wt% NaCl solution to investigate the anticorrosive properties.

Fig. 7 represents the Nyquist plots for the uncoated and ORMOSIL-ZrO_2 hybrid nanocomposites coated aluminium alloy substrates at the time of immersion in NaCl solution. The dimension of the semicircle loop has increased considerably for the ORMOSIL-ZrO_2 hybrid nanocomposite coatings compared to the uncoated aluminium alloy substrate, which is attributed to a lower corrosion rate.[49] Table 3 summarizes the electrochemical corrosion results of the ORMOSIL-ZrO_2 hybrid nanocomposite coatings. The ORMOSIL-ZrO_2 hybrid composition, HNC-Zr-0.5 coated aluminium alloy, has an enhanced corrosion protection when compared to that of bare aluminium alloy and other compositions as evidenced from a low corrosion current of 0.5837 µA and a high charge transfer resistance of 22462.3 Ω.

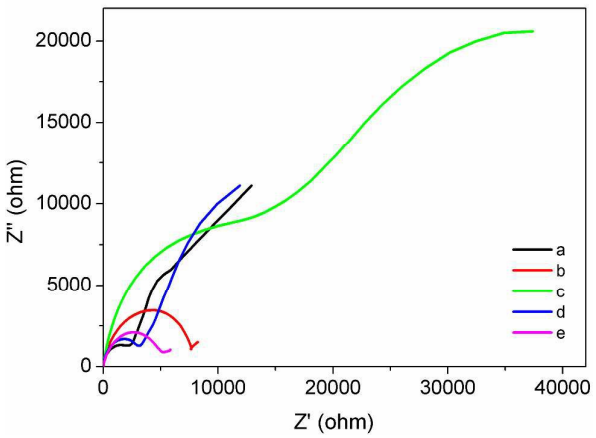

Fig. 7. Nyquist plot for the (a) uncoated (b) HNC-Zr-0 (c) HNC-Zr-0.5 (d) HNC-Zr-1 and (e) HNC-Zr-2 hybrid nanocomposite coated Al alloy substrates, all calcined at 400 °C.

Table 3. Summary of the electrochemical parameters obtained from the polarization measurements in 3.5 wt% NaCl solution.

Samples coated on Aluminium Alloy	Electrochemical corrosion measurements (Immersion time – 0h)						
	E_{corr} (V)	I_{corr} (µA)	β_A (V)	β_C (V)	R_{ct} (Ω)	R_p (Ω)	Corrosion Rate (mpy)
Uncoated	-0.832	0.8069	11.262	4.859	3245.5	1.8266	0.3492
HNC-Zr-0	-0.959	1.773	36.670	7.902	8217.2	1.5921	0.7674
HNC-Zr-0.5	-0.984	**0.5837**	4.838	5.716	**22462.3**	1.9492	0.2526
HNC-Zr-1	-1.138	0.8677	5.140	7.043	3526.7	1.4869	0.3755
HNC-Zr-2	-1.234	4.426	0.2623	6.209	5424.4	0.0246	1.9158

E_{corr}-corrosion potential, I_{corr}-corrosion current, β_A and β_C anodic and cathodic slopes, R_{ct} -charge transfer resistance, R_p -polarization resistance.

Also, the corrosion rate for the HNC-Zr-0.5 coated aluminium alloy was lower (0.2526 mpy) when compared to that of other samples. An enhanced corrosion protection is usually indicated by higher corrosion potential (E_{corr}), charge transfer resistance (R_{ct}) and polarization resistance (R_p) and a lower corrosion current (I_{corr}) value.[50] A charge transfer resistance of 7100 Ω was reported for a clay-polystyrene nanocomposite coating on aluminium alloy by Raju et al.[51] that offered a high corrosion resistant property to the alloy. The charge transfer resistance of the ORMOSIL-ZrO_2-hybrid nanocomposite coating on aluminium alloy in the present work is much higher than the clay polystyrene nanocomposite coatings thereby providing enhanced corrosion resistance features.

However, the corrosion potential values obtained for the hybrid nanocomposite coatings as evident from the Tafel plots (Fig. 8) was more negative compared to that of the bare substrate which indicates that the coatings are less corrosion resistant. These results are contradictory to the corrosion rate and corrosion current results which shows lowered value indicating their high corrosion resistance. A similar behaviour was already reported by Qingyang Li et al. for the nanocrystalline zinc oxide coatings on metals in which they explain this contradiction of lower corrosion potential and higher corrosion resistance is due to the intrinsic electrochemical behaviour of the coated material.[52] The intrinsic electrochemical behaviour of a material is largely reflected by its electron work function (EWF), which is the minimum energy required to extract electron from inside a solid to its surface without kinetic energy.[52]

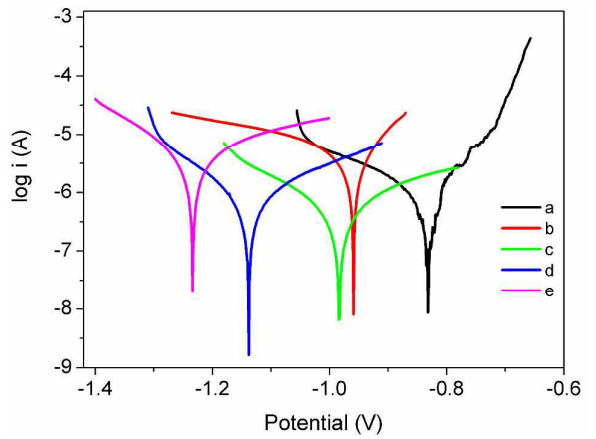

Fig. 8. Tafel plot for the (a) uncoated (b) HNC-Zr-0 (c) HNC-Zr-0.5 (d) HNC-Zr-1 and (e) HNC-Zr-2 hybrid nanocomposite coated aluminium alloy substrates, all calcined at 400 °C at the time of immersion in NaCl solution.

EWF is a measure of intrinsic proneness of a material to corrosion and a lower EWF corresponds to a higher tendency of electrons for participating in corrosion reactions. Zirconium oxide is known for its low EWF (~2.8 eV)[53, 54] and hence the electrons at the surface of the nanocrystalline coating are not confined and are more active which makes it easy to enter easily into the NaCl solution and participate in the electrode

View Article Online
DOI: 10.1039/C7NJ05174C

reaction resulting in corrosion. The formed insoluble corrosion product layer on surface of the nanocrystalline coating inhibits further corrosion leading to a decrease in the corrosion rate.[52]

The electrochemical measurements were also carried out for the uncoated and HNC-Zr-0.5 coated aluminium alloy (annealed at 400 °C) in 3.5 wt% NaCl solution for an immersion time of 1h and the results are presented in Fig. 9. From the Nyquist plots, the dimension of the semicircle loop has increased drastically for the HNC-Zr-0.5 coating compared to the uncoated aluminium alloy substrate, further proving the increased corrosion resistance of the hybrid nanocomposite coating even after immersing the coated substrate in NaCl for 1h.

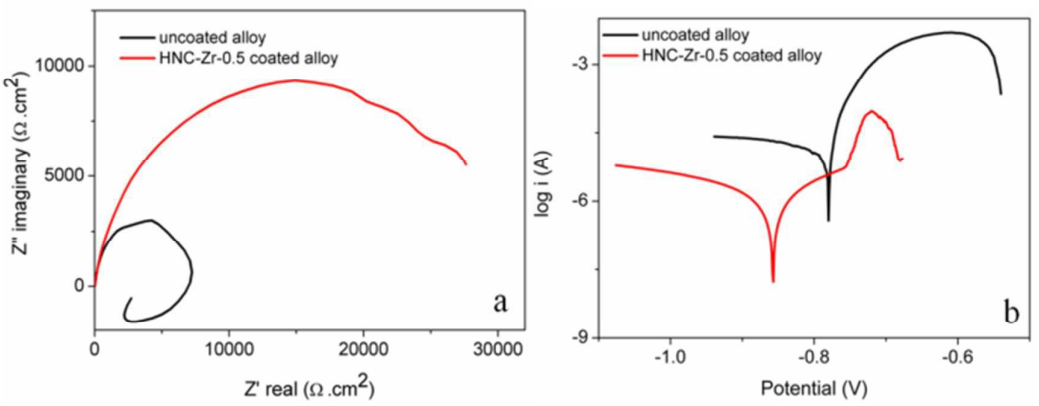

Fig. 9. (a) Nyquist plot and (b) Taffel Plots for the uncoated and HNC-Zr-0.5 hybrid nano-composite coated aluminium alloy (400 °C annealed) after 1h immersion in 3.5 wt% NaCl.

For the uncoated substrate, a capacitive loop followed by an inductive loop at low frequency was observed. The low frequency inductive behaviour is reported to be an adsorption process at the electrode surface leading to pitting corrosion.[55] Keddam et al. has attributed this inductive loop at low frequencies to the weakening of the protective effectiveness of the aluminium oxide layer due to anodic dissolution of the alloy.[56] Taffel plot shows contradictory behaviour here also which can be explained due to the low EWF of zirconium oxide present in the ORMOSIL matrix here. Table 4 summarizes the electrochemical corrosion measurements of the uncoated and the HNC-Zr-0.5 coating for an immersion time of 1h in 3.5 wt% NaCl. HNC-Zr-0.5 coated aluminium alloy has got an enhanced corrosion protection when compared to that of bare aluminium alloy as evidenced from a low corrosion current (0.989 µA) and a high charge transfer resistance (32488.14 Ω) and lower corrosion rate (0.4280 mpy). Thus from the electrochemical studies, the hybrid nanocomposite HNC-Zr-0.5 was found as the optimum composition among the different hybrid nanocomposites synthesized in the present study. Rosero-Navarro et al[57] has reported an Rct value of 3600 Ω (immersion time – 1h) for the cerium containing sol–gel coatings reinforced with SiO_2 nanoparticles which provides anticorrosive protection for AA2024 alloy. The Rct of HNC-Zr-0.5 hybrid nanocomposite coating after 1h immersion in NaCl in the present study is much higher indicating good corrosion resistance features.

Also, the corrosion rate for an uncoated aluminium alloy after immersion in NaCl for 1h has increased drastically (~85 times) when compared with the uncoated sample immersed for only 0 h. On the other hand, the corrosion rate for HNC-Zr-0.5 coated aluminium alloy after immersion in NaCl for 1h has increased only marginally (~1.6 times) when compared with the coated sample immersed only for 0h.

Table 4. Summary of the electrochemical parameters obtained from the corrosion studies in 3.5 wt % NaCl solution (1h immersion).

Samples coated on Aluminium Alloy	Electrochemical corrosion measurements (Immersion time -1h)						
	E_{corr} (V)	I_{corr} (µA)	β_A (V)	β_C (V)	R_{ct} (Ω)	R_p (Ω)	Corrosion Rate (mpy)
Uncoated	-0.780	69.93	9.244	1.854	7516.424	0.0958	30.2693
HNC-Zr-0.5	-0.857	**0.989**	14.428	4.037	**32488.143**	1.3849	**0.4280**

The significant difference between the electrochemical parameters for the uncoated and coated aluminium alloy indicates that the ORMOSIL-ZrO_2 hybrid nanocomposite has great potential towards developing anticorrosive coatings. The optical transmittance of the prepared coatings on glass substrates were measured further in order to evaluate the suitability of the material as functional coatings where high optical clarity is essential and the results are given in Fig. 10.

View Article Online
DOI: 10.1039/C7NJ05174C

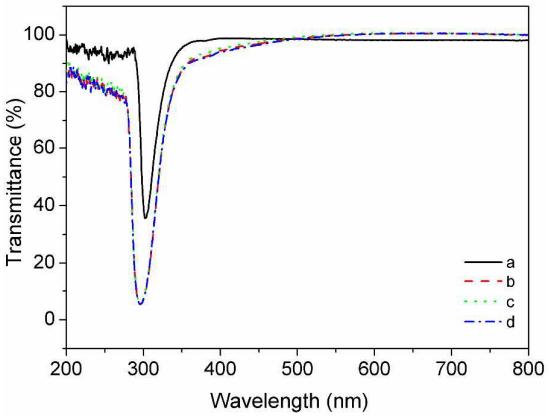

Fig. 10. UV-Visible transmittance of ORMOSIL-ZrO_2 hybrid nanocomposite coatings (a) HNC-Zr-0 (b) HNC-Zr-0.5 (c) HNC-Zr-1 and (d) HNC-Zr-2, all annealed at 400 °C.

All the hybrid nanocomposite coatings containing ZrO_2 were highly transparent in the visible region of the UV-spectra which indicates that these thin functional coatings can be made on different substrates without affecting their aesthetic appeal. The morphological features of the ORMOSIL-ZrO_2 hybrid nanocomposite coating (HNC-Zr-0.5) prepared on glass substrate annealed at 400 °C is provided below in Fig. 11.

SEM surface image of the hybrid nanocomposite coating on the glass substrate also shows the presence of porosity in the coating with an average pores size of ~50 nm. The coatings prepared on the glass substrate had a thickness of ~3 µm as is clear from Fig. 11 b.

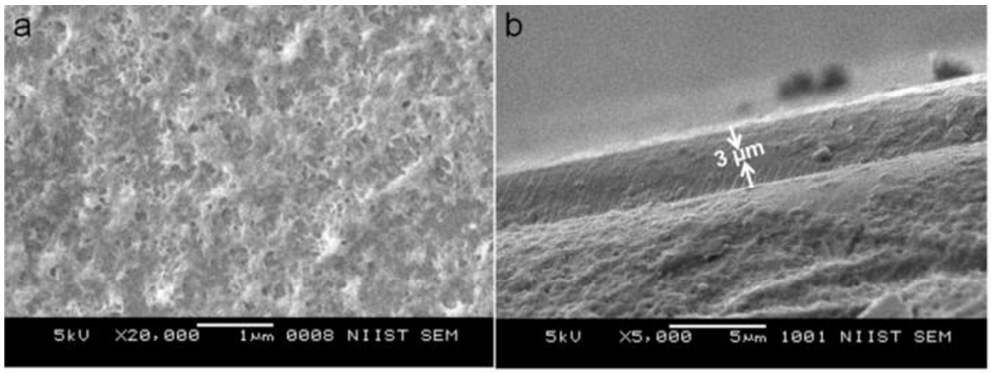

Fig. 11. SEM surface images of (a) HNC-Zr-0.5 nanocomposite powder calcined at 400 °C (b) HNC-Zr-0.5 nanocomposite coating on glass substrate annealed at 400 °C (c) EDX of (a) and (d) thickness image of HNC-Zr-0.5 nanocomposite coating annealed at 400 °C.

AFM image of the hybrid nanocomposite coating on the glass substrate (annealed at 400 °C) is presented in Fig. 12. The results obtained from AFM agree with the SEM results, indicating porous surface structure with varying pore size in the range 50-100 nm. The surface is covered with similar sized ORMOSIL clusters with an average size of ~50 nm and had a surface roughness of ~18 nm.

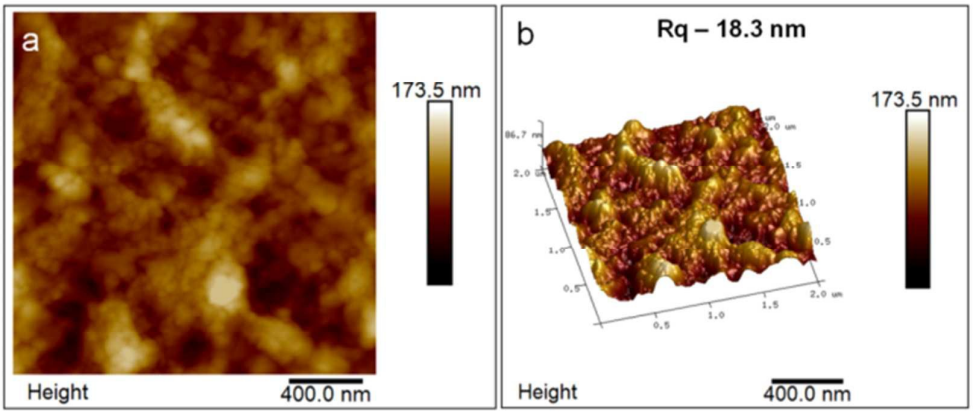

Fig. 12. AFM images of HNC-Zr-0.5 nanocomposite coating on glass annealed at 400 °C (a) surface image (b) 3D image.

Fig. 13 shows the SEM image, corresponding elemental mapping and the coating thickness of the ORMOSIL-ZrO_2 hybrid nanocomposite coating on the aluminium alloy substrate.

View Article Online
DOI: 10.1039/C7NJ05174C

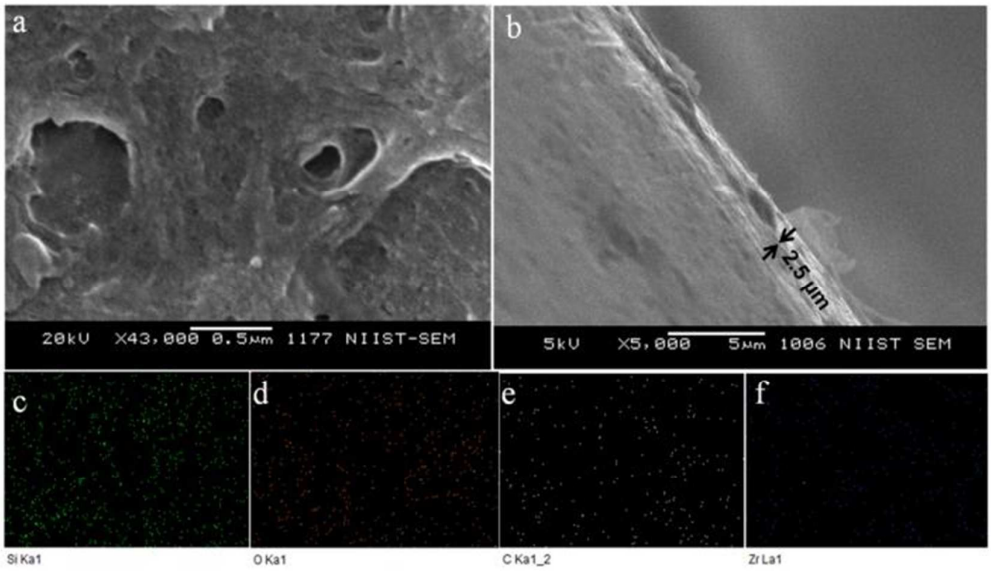

Fig. 13. SEM image of HNC-Zr-0.5 hybrid nanocomposite coating on aluminium alloy substrate annealed at 400 °C (a) showing surface morphology (b) showing coating thickness and (c-f) distribution of elements such as Si, O, C and Zr on the surface of coating.

SEM image indicates that the coating is porous (average pore size ~50 nm) with a thickness of ~2.5 µm. The elemental mapping of the coated substrate shows that zirconia is uniformly distributed all over the silica matrix. Fig. 14 shows the AFM images of the hybrid nanocomposite coatings (HNC-Zr-0.5) on aluminium alloy substrate annealed at 400 °C.

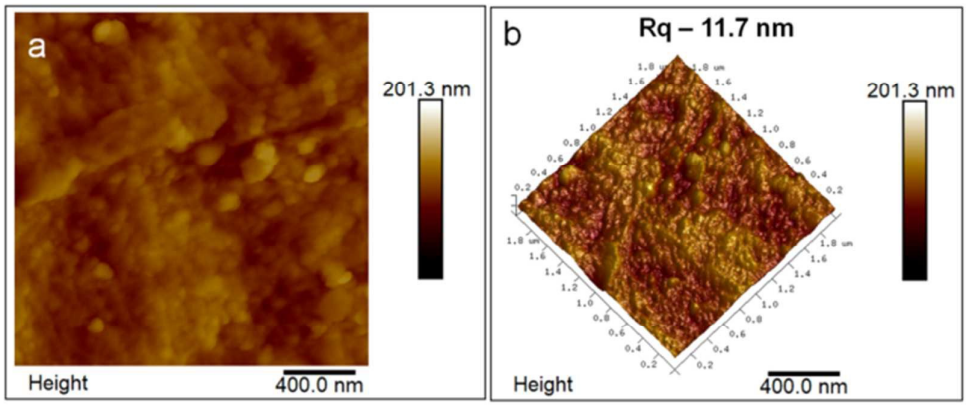

Fig. 14. AFM image of HNC-Zr-0.5 hybrid nanocomposite coating on aluminium alloy substrate annealed at 400 °C (a) surface image (b) 3D image.

The surface is covered with ORMOSIL clusters with an average size of ~50-100 nm and had a surface roughness of ~11 nm. The porous surface structure (pore size ~50-100 nm) of the coating is also clear from the image. The high transparency of the hybrid nanocomposite coatings in the present study can be attributed to the low surface roughness values.[58] Thus the hybrid nanocomposite, HNC-Zr-0.5 coated substrates possess anticorrosive properties and are transparent which makes them an important candidate in the field of functional protective environment resistant or decorative coatings.

Conclusions

ORMOSIL-ZrO_2 hybrid nanocomposite aerogel monoliths and coatings were successfully prepared by a sol-gel methodology involving gelation of the organosilane precursors of methyltrimethoxysilane and glycidyloxypropyltrimethoxysilane with zirconium isopropoxide. A series of hybrid nanocomposites were prepared by varying the amount of zirconia precursor, which showed reasonable surface areas in the range of 329-359 m^2/g and pore diameters of ~2 nm. ORMOSIL-ZrO_2 hybrid nanocomposite coatings were also prepared on substrates such as aluminium alloy and glass followed by annealing at 400 °C. HNC-Zr-0.5 coated aluminium alloy has an enhanced corrosion protection when compared to that of bare aluminium alloy and other compositions as evidenced from a low corrosion current of 0.5837 µA, a high charge transfer resistance of 22462.3 Ω and a

View Article Online
DOI: 10.1039/C7NJ05174C

low corrosion rate of 0.2526 mpy. HNC-Zr-0.5 coated aluminium alloy and an uncoated aluminium alloy were further subjected to corrosion studies for 1h immersion time in 3.5 wt% NaCl and the results showed that an uncoated substrate is characterized by a high corrosion current of 69.93 µA, a very low charge transfer resistance of 7516.4 Ω and a high corrosion rate of 30.2693 mpy whereas the HNC-Zr-0.5 coated substrate was highly corrosion resistant evidenced by a low corrosion current of 0.989 µA, a high charge transfer resistance of 32488.14 Ω and a low corrosion rate of 0.4280 mpy. The hybrid nanocomposite coatings are porous with an average pore size of ~50 nm with uniform distribution of Zr in the ORMOSIL matrix and possess very good transparency (~99.9 %). The functional features such as transparency and anticorrosive properties of the ORMOSIL-ZrO_2 hybrid nanocomposite coating (HNC-Zr-0.5) makes them an important candidate in the field of functional protective environment resistant or decorative coatings.

Experimental

Materials

Methyltrimethoxysilane (MTMS, 98%) and (3-glycidyloxypropyl)trimethoxysilane (GPTMS, 98%), the silane precursors and zirconium isopropoxide (ZIP - 70 wt% in 1-propanol) were purchased from Sigma-Aldrich (U. S.) and were used as purchased. Methanol (Emparta®), ammonium hydroxide (25 %, Emparta®) and ammonium fluoride were purchased from Merck Chemicals Pvt. Ltd., India. LR grade Oxalic acid was used for the hydrolysis (Qualigens Pvt. Ltd., India). Aluminium alloy substrates (4 cm x 2.5 cm x 0.25 cm), A 6061 alloy was used for coating the hybrid compositions which had ~98 % Al content. Microscopic glass slides were also used for the coating purpose.

Methods

Hybrid nanocomposite aerogels were prepared by a two-step acid-base catalysis mechanism.[11] The organo silane precursors MTMS and GPTMS were hydrolyzed in presence of methanol under acidic conditions. MTMS, GPTMS, methanol and 0.001 M oxalic acid were mixed in the molar ratio 1: 0.5: 35: 8 and was allowed to stir for 24 h for complete hydrolysis of the silane precursors. ZIP was then added drop wise to the silica sol to get the hybrid nanocomposite sol where the ratio of MTMS: ZIP was 1: 0.5, 1: 0.7 and 1: 1. A blank composition without ZIP was also prepared for comparison. The hybrid nanocomposite sols were stirred for 1h. The condensation reaction was carried out further by the addition of basic catalyst (6.5 M NH_4OH and 1M NH_4F) in a molar ratio 1: 0.1 with respect to MTMS. Viscosity and pH of the hybrid nanocomposite sols with respect to condensation reaction was measured. The synthesized sols have transformed to their corresponding gels and the time required for complete gelation of the sols were also found out. The synthesized gels were aged in methanol for one day and homogenized, by using an ultrasonic liquid homogenizer, for 20 minutes at 750 W. The homogenized solution was dip coated at a rate 20 mm per minute on microscopic glass slides and aluminium alloy substrates. The glass substrates were cleaned in soap solution and washed with acetone prior to coating. The aluminium substrates were polished using various grade sand papers (120, 220, 400, 600 and 800 grit sizes). The polished aluminium alloy substrates are then ultrasonicated for 10 min in acetone, washed thoroughly in distilled water and further immersed in 1 % NaOH and in 20 % HNO_3 (2 min each). The polished substrates were further washed in distilled water and were dried using an air dryer.

The prepared hybrid nanocomposite coatings were dried at room temperature for complete evaporation of the remaining solvent. The hybrid nanocomposite aerogels and coatings were named as "HNC-Zr-X" where 'HNC' indicates hybrid nanocomposite aerogel, 'X' represents the mol fraction of ZIP. The dried coatings were further annealed at 400 ºC for 1 h.

The obtained wet alcogels were finally dried under ambient conditions for about seven days to get hybrid nanocomposite aerogel monoliths which were further calcined at 400 ºC for 1h. The hybrid nanocomposite aerogels were further characterised for its surface area (BET), crystallinity and morphological features.

The viscosity of the sol was measured using an Anton Paar Modular Compact Rheometer. The BET (Brunauer, Emmett and Teller) surface area measurements and pore size analysis of the hybrid aerogels were carried out by nitrogen adsorption using a Micromeritics Gemini 2375 surface area analyzer after degassing each sample at 150-200 °C for 2 hours. Wide- angle X-ray scattering (WAXS) measurements were performed using XEUSS SAXS/ WAXS system by Xenocs, operated at 50 kV and 0.60 mA in the 2θ range 5–35 ° using Cu Kα radiation (λ = 1.54 Å). Infrared spectra were recorded in a Bruker FTIR spectrometer, in the range 4000–400 cm^{-1} on the samples, dispersed in KBr pellets (2–3% sample-KBr dilution). X-ray photoelectron spectroscopic study was carried out using PH1 5000 Versa Probe II spectrometer to analyse the chemical state, structure and bonding states of the hybrid nanocomposite. Sample mounting for XPS analysis was done by fixing the powder sample in the holder using an adhesive tape. All spectra were referenced against the C1s peak at 285 eV to correct for charging effects during acquisition. An XPS related software XPSPEAK 4.1 was used for peak fitting analysis using Guassian function. Quantitative surface chemical analyses were done by following the removal of a non-linear (Shirley) background from the spectra. Morphology of the hybrid nanocomposite aerogels and coatings were observed using a scanning electron microscope (SEM) (JEOL JSM-5600LV), Japan operated at 5-10 kV. Atomic force microscopy (AFM) measurements were used for ascertaining the surface roughness and morphology of the coated surfaces. AFM images (Tapping-mode) were recorded by using a Bruker multimode 8 AFM. The transmittance of the coated samples (on glass) was

View Article Online
DOI: 10.1039/C7NJ05174C

recorded using a Shimadzu UV 2401 PC spectrophotometer (spectral range 200–800 nm). The transmittance values were normalized by taking the uncoated glass of the same type as the reference.

Electrochemical measurements of the hybrid nanocomposite coated Aluminium alloy (3 times coated) were carried out further. Potentiodynamic polarization and electrochemical impedance measurements were conducted in an electrochemical system (CH Instruments Inc., Model 680A) with three electrode cells of saturated calomel electrode (SCE) as reference electrode, a platinum mesh as counter electrode, and the sample as working electrode. All electrochemical experiments were carried out at room temperature (25±1 °C) with 3.5 wt % NaCl solution as electrolyte. The surface area of the sample exposed to the electrolyte was 1 cm^2. The samples were immersed in the electrolyte for 20 min to monitor their open circuit potential (OCP) till they reached a relatively stable value. The samples were scanned from cathodic region to anodic region at a rate of 1 mV/s, in the range of -200 mV to +300 mV with reference to their corresponding OCP values. The corrosion current (I_{corr}) and corrosion potential (E_{corr} vs. SCE) were measured from the Tafel plot. The impedance measurements on the samples were performed at their open circuit potential with a peak-to-peak amplitude of 5 mV in the frequency range from 10^4 to 10^{-2} Hz. Similarly electrochemical experiments were carried out in 3.5 wt% NaCl for an immersion time of 1h also. The corrosion potential (E_{corr}), anodic and cathodic Tafel slopes (β_A and β_C) and the corrosion current (I_{corr}) can be determined using polarization curves obtained from CHI 680 software. The corrosion rate and polarization resistances were also determined further.

Conflicts of interest

There are no conflicts to declare.

Acknowledgements

The authors acknowledge Ms. R. Remya for electrochemical characterizations. Mr. Harish, Mr. Kiran and Mr. Vibu Darshan are being acknowledged for SEM, TEM and AFM analysis respectively. Authors thank the members of Materials Science and Technology Division for providing general assistance. The author Smitha V. S. is grateful to CSIR, India, for providing financial support.

References

1. M. R. Pai, A. M. Banerjee, A. K. Tripathi and S. R. Bharadwaj, in *Functional Materials*, Elsevier, London, 2012, pp. 579-606.
2. J. A. Kilner, S. J. Skinner, S. J. C. Irvine and P. P. Edwards, *Functional Materials for Sustainable Energy Applications*, Elsevier Science, 2012.
3. C. Sanchez, B. Julian, P. Belleville and M. Popall, *J. Mater. Chem.*, 2005, **15**, 3559.
4. Y. Joshua Du, M. Damron, G. Tang, H. Zheng, C. J. Chu and J. H. Osborne, *Prog. Org. Coat.*, 2001, **41**, 226.
5. I. J. Zvonkina and M. D. Soucek, *Curr. Opin. Chem. Eng.*, 2016, **11**, 123.
6. H. Schmidt, *The Journal of Adhesion*, 1987, **22**, 77-80
7. J. D. Mackenzie and E. P. Bescher, *J. Sol-Gel Sci. Technol.*, 1998, **13**, 371.
8. G. Kickelbick, *Prog. Polym. Sci.*, 2003, **28**, 83-114.
9. B. Domenech, I. Mata and E. Molins, *RSC Adv.*, 2016, **6**, 10736.
10. L. Merhari, *Hybrid Nanocomposites for Nanotechnology: Electronic, Optical, Magnetic and Biomedical Applications*, Springer US, 2009.
11. H. Budunoglu, A. Yildirim, M. O. Guler and M. Bayindir, *ACS Appl. Mater. Interfaces*, 2011, **3**, 539.
12. T. L. Metroke and A. Apblett, *Prog. Org. Coat.*, 2004, **51**, 36.
13. R. L. Parkhill, E. T. Knobbe and M. S. Donley, *Prog. Org. Coat.*, 2001, **41**, 261.
14. R. Figueira, I. Fontinha, C. Silva and E. Pereira, *Coatings*, 2016, **6**, 12.
15. V. Dalmoro, J. H. Z. dos Santos, C. Alemán and D. S. Azambuja, *Corros. Sci.*, 2015, **92**, 200.
16. Y. T. Caballero, E. A. Rondón, L. Rueda, C. A. H. Barrios, A. Coy and F. Viejo, *J. Phys. Conf. Ser.*, 2016, **687**, 012014.
17. C.-Y. Li, J. Y. Tseng, K. Morita, C. L. Lechner, Y. Hu and J. D. MacKenzie, *ORMOSILS as matrices in inorganic-organic nanocomposites for various optical applications*, 1992.
18. G. Tsaneva, V. Kozhukharov, S. Kozhukharov, M. Ivanova, J. Gerwann, M. Schem and T. Schmidt, *Functional Nanocomposite Coatings for Corrosion Protection of Aluminium Alloy and Steel*, 2008.
19. V. Dalmoro, J. H. Z. dos Santos, E. Armelin, C. Alemán and D. S. Azambuja, *J. Colloid Interface Sci.*, 2014, **426**, 308.
20. J. Figueroa-Lara, M. Torres-Rodríguez, M. Gutiérrez-Arzaluz and M. Romero-Romo, *Materials*, 2017, **10**, 1135.
21. J. B. Ruiz, W. Aperador and J. C. Gómez, *J. Phys. Conf. Ser.*, 2016, **687**, 012031.
22. V. Dalmoro, C. Santos and J. H. Z. dos Santos, *Smart coatings for corrosion protection," in Industrial Applications for Intelligent Polymers and Coatings*, Springer International Publishing, 2016.
23. E. Bescher and J. D. Mackenzie, *J. Sol–Gel Sci. Technol.*, 2003, **26**, 1223.
24. H. Wang, J. Ding, Y. Xue, X. Wang and T. Lina, *J. Mater. Res.*, 2010, **25**, 1336.
25. V. S. Smitha, P. M. A. Azeez, K. G. Warrier, B. N. Nair and U. N. S. Hareesh, *ChemistrySelect*, 2018, **3**, 2989.
26. K. Sinkó, *Materials*, 2010, **3**, 704.
27. C. J. Brinker and G. W. Scherer, *Sol-Gel Science: The Physics and Chemistry of Sol-Gel Processing*, Elsevier Science, 2013.
28. Y. Hoshino and J. D. Mackenzie, *J. Sol-Gel Sci. Technol.*, 1995, **5**, 83.
29. E. P. Ferreira-Neto, S. Ullah, F. L. S. de Carvalho, A. L. de Souza, M. de Oliveira, J. F. Schneider, Y. P. Mascarenhas, A. M. Jorge and U. P. Rodrigues-Filho, *Mater. Chem. Phys.*, 2015, **153**, 410.
30. X. Rios, P. Moriones, J. C. Echeverría, A. Luquin, M. Laguna and J. J. Garrido, *Mater. Chem. Phys.*, 2013, **141**, 166.
31. J. C. Echeverría, J. J. Garrido, M. Laguna, A. Luquin, P. Moriones and X. Rios, *Adsorption*, 2011, **17**, 583.
32. S. C. Pillai and S. Hehir, *Sol-Gel Materials for Energy, Environment and Electronic Applications*, Springer International Publishing, 2017.
33. S. N. Basahel, T. T. Ali, M. Mokhtar and K. Narasimharao, *Nanoscale res. Let.*, 2015, **10**, 73.

View Article Online
DOI: 10.1039/C7NJ05174C

34. A. A. S. Alfaya and Y. Gushikem, *J. Colloid Interface Sci.*, 1999, **209**, 428.
35. E. R. Lippincott, A. V. Valkenburg, C. E. Weir and E. N. Bunting, *J. Res. Natl. Bur. Stand.,* 1958, **61**, 61.
36. G. Ambrosone, D. K. Basa, U. Coscia, L. Santamaria, N. Pinto, M. Ficcadenti, L. Morresi, L. Craglia and R. Murri, *Energy Procedia*, 2010, **2**, 3.
37. S. M. Hwang, J. H. Choi, S. M. Lee, J. H. Lim and J. Joo, *The J. Phys. Chem. C*, 2012, **116**, 11386.
38. W. W. Anku, S. O.-B. Oppong, S. K. Shukla, E. S. Agorku and P. P. Govender, *Progress in Natural Science: Materials International*, 2016, **26**, 354.
39. J. J. H. Lancastre, N. Fernandes, F. M. A. Margaça, I. M. Miranda Salvado, L. M. Ferreira, A. N. Falcão and M. H. Casimiro, *Radiat. Phys. Chem.*, 2012, **81**, 1336.
40. Z. Dang, B. G. Anderson, Y. Amenomiya and B. A. Morrow, *J. Phys. Chem.*, 1995, **99**, 14437.
41. M. Oubaha, P. C. R. Varma, B. Duffy, Z. M. Gasem and S. J. Hinder, *Advances in Materials Physics and Chemistry*, 2014, **4**, 10.
42. P. J. Timans, *Advanced Gate Stack, Source/Drain, and Channel Engineering for Si-Based CMOS 4,* Electrochemical Society, 2008.
43. B. N. Sahoo, N. S. K. Gunda, S. Nanda, J. A. Kozinski and S. K. Mitra, *ACS Sustainable Chem. Eng.*, 2017, **5**, 6716.
44. S. Y. Moon, *J. Phys. Sci. Appl.*, 2016, **6**, 29.
45. L.-G. Kim, H.-G. Park, Y.-H. Kim and D.-S. Seo, *IEEE Electron Device Lett.*, 2012, **33**.
46. D. L. Kwong, *Rapid Thermal and Other Short-time Processing Technologies II: Proceedings of the International Symposium*, Electrochemical Society, 2001.
47. S. N. Basahel, T. T. Ali, M. Mokhtar and K. Narasimharao, *Nanoscale Res. Lett.*, 2015, **10**, 73.
48. X. Gao, J. L. G. Fierro and I. E. Wachs, *Langmuir*, 1999, **15**, 3169.
49. H.-S. Lee, J. Singh, M. Ismail and C. Bhattacharya, *Metals*, 2016, **6**, 55.
50. A. Ganash, *Int. J. Electrochem. Sci.*, 2014, **9** 4000.
51. A. Raju, V. Lakshmi, R. K. Vishnu Prataap, V. G. Resmi, T. P. D. Rajan, C. Pavithran, V. S. Prasad and S. Mohan, *Appl. Clay Sci.*, 2016, **126**, 81.
52. Q. Li, H. Lu, J. Cui, M. An and D. Li, *RSC Adv.*, 2016, **6**, 97606.
53. R. F. Egerton, *Physical Principles of Electron Microscopy: An Introduction to TEM, SEM, and AEM*, Springer International Publishing, 2016.
54. H. Nakanea, S. Satoh and H. Adachi, *Journal of Vacuum Science & Technology B, Nanotechnology and Microelectronics: Materials, Processing, Measurement, and Phenomena* 2005, **23**, 769.
55. Z. Szklarska-Smialowska, *Corros. Sci.*, 1992, **33**, 1193.
56. M. Keddam, C. Kuntz, H. Takenouti, D. Schustert and D. Zuili, *Electrochim. Acta*, 1997, **42**, 87.
57. N. C. Rosero-Navarro, S. A. Pellice, A. Dura´n and M. Aparicio, *Corros. Sci.*, 2008, **50**, 1283.
58. V. S. Smitha, K. Vidya, M. Jayasankar, A. Peer Mohamed, U. S. Hareesh and K. G. K. Warrier, *RSC Adv.*, 2016, **6**, 31114.

View Article Online
DOI: 10.1039/C7NJ05174C

Ormosil-ZrO_2 hybrid nanocomposites and coatings on aluminium alloy for corrosion resistance; A sol-gel approach

V. S. Smitha,[a]* S. S. Syamili,[a] A. Peer Mohammed,[a] Balagopal N Nair [b,c] and U. S. Hareesh*[a,d]

Sol-gel derived ORMOSIL-ZrO_2 hybrid nanocomposites as protective environment resistant functional coatings on glass substrate and aluminium alloys.

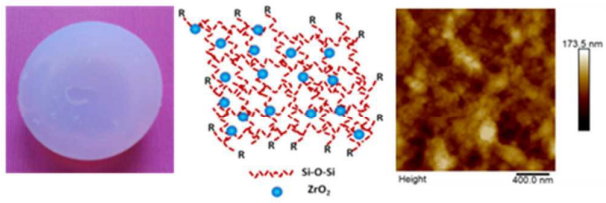

Porous ORMOSIL-ZrO_2 nanocomposite aerogel monolith and coatings